Micro-pulling-down growth of long YAG- and LuAG-based garnet fibres: advances and bottlenecks

O. Sidletskiy, K. Lebbou, D. Kofanov

▶ **To cite this version:**

O. Sidletskiy, K. Lebbou, D. Kofanov. Micro-pulling-down growth of long YAG- and LuAG-based garnet fibres: advances and bottlenecks. CrystEngComm, 2021, 23 (14), pp.2633-2643. ⟨10.1039/D1CE00091H⟩. ⟨hal-03227689⟩

HAL Id: hal-03227689

https://hal.science/hal-03227689v1

Submitted on 8 Nov 2021

HAL is a multi-disciplinary open access archive for the deposit and dissemination of scientific research documents, whether they are published or not. The documents may come from teaching and research institutions in France or abroad, or from public or private research centers.

L'archive ouverte pluridisciplinaire **HAL**, est destinée au dépôt et à la diffusion de documents scientifiques de niveau recherche, publiés ou non, émanant des établissements d'enseignement et de recherche français ou étrangers, des laboratoires publics ou privés.

HAL Authorization

Check for updates

View Article Online
View Journal

CrystEngComm

Accepted Manuscript

This article can be cited before page numbers have been issued, to do this please use: O. Sidletskiy, K. Lebbou and D. Kofanov, *CrystEngComm*, 2021, DOI: 10.1039/D1CE00091H.

This is an Accepted Manuscript, which has been through the Royal Society of Chemistry peer review process and has been accepted for publication.

Accepted Manuscripts are published online shortly after acceptance, before technical editing, formatting and proof reading. Using this free service, authors can make their results available to the community, in citable form, before we publish the edited article. We will replace this Accepted Manuscript with the edited and formatted Advance Article as soon as it is available.

You can find more information about Accepted Manuscripts in the Information for Authors.

Please note that technical editing may introduce minor changes to the text and/or graphics, which may alter content. The journal's standard Terms & Conditions and the Ethical guidelines still apply. In no event shall the Royal Society of Chemistry be held responsible for any errors or omissions in this Accepted Manuscript or any consequences arising from the use of any information it contains.

ROYAL SOCIETY OF CHEMISTRY

rsc.li/crystengcomm

View Article Online
DOI: 10.1039/D1CE00091H

Micro-pulling-down growth of long YAG- and LuAG-based garnet fibres: advances and bottlenecks

O. Sidletskiy,[1,*] K. Lebbou,[2] D. Kofanov[1]

[1]Institute for Scintillation Materials NAS of Ukraine, 60 Nauky Ave., 61072, Kharkiv, Ukraine

[2]Institut Lumière Matière UMR 5306, Université Lyon, Université Claude Bernard Lyon 1, CNRS, 69100, Villeurbanne, France

*Corresponding author e-mail: sidletskiy@isma.kharkov.ua, osidletskiy@yahoo.com

Published on 04 March 2021. Downloaded by Université Claude Bernard Lyon on 3/10/2021 9:05:29 AM.

CrystEngComm Accepted Manuscript

Abstract

New high energy experiments at colliders raise the demand for cheap and radiation-hard detector materials capable to mass production. The concepts of new generation of high energy physics experiments include combined electromagnetic and hadron calorimeters for simultaneous detection of scintillation and Cherenkov emission by undoped and lanthanide-doped crystalline fibres. Micro-pulling-down (μ-PD) method provides the growth of long single crystalline fibres in ready-to-use shape without a need of further cutting and polishing. In this highlights paper the recent achievements in μ-PD growth of long $Y_3Al_5O_{12}$ (YAG)- and $Lu_3Al_5O_{12}$ (LuAG)-based fibres in Institute of Light and Matter are reviewed. Optimization of Ce concentration, pulling rate, crystallizer configuration resulted in the obtaining of highly transparent LuAG:Ce fibres with the light attenuation length of up to 1 m. Meanwhile, such an excellent transparency has not been reproduced in YAG:Ce fibers. The main differences in the crystallization processes of YAG- and LuAG-based fibres are discussed in connection with their physical properties. The paper also addresses codoping of garnet fibres by Mg^{2+} ions and growth from non-stoichiometric melts to adjust fiber transmission and scintillation performance.

View Article Online
DOI: 10.1039/D1CE00091H

Published on 04 March 2021. Downloaded by Université Claude Bernard Lyon on 3/10/2021 9:05:29 AM.

1. Introduction

An excellent operation of CMS electromagnetic calorimeter at CERN based on $PbWO_4$ (PWO) contributed to the discovery of Higgs boson [1]. Meanwhile, increasing dose loads in colliders call the need to substitute PWO with lighter scintillators suffering less radiation damage owing to the interaction with high energy hadrons [2]. Construction of FAIR calorimeter, announcement of the upgraded Large Hadron Collider (HL-LHC) [3], modernization of LHCb calorimeter, and intense development of International Linear Collider program [4] rise demands for cheap and radiation-hard materials capable to mass production. Meanwhile, the concepts of new generation of high energy physics (HEP) experiments include combined electromagnetic and hadron calorimeters for simultaneous detection of scintillation and Cherenkov emission by undoped and lanthanide-doped crystalline fibres with the 1-6 mm^2 cross section [5-10].

The fibre-shaped detector cost is a key problem since a huge amount of fibres is required in calorimeters. Producing fibres from large crystals grown by the Czochralski, or other methods of bulk crystal growth is relatively expensive because of material loss during cutting and polishing stages. Furthermore, technologies of growing uniform bulk crystals of the required size (10-25 cm) are not always available. The micro-pulling-down (μ-PD) method is one of the efficient methods of growing single crystalline fibres with a prescribed shape and length without further machining. This method provides fabrication of single crystalline rods of controlled shape [11-13] with the cross section of up to ca. 9 mm^2. Crystallization of nearly 100 % of the melt in the crucible is an additional advantage, as in the Czochralski process the crystallized melt deforms the crucible during cooling [14]. μ-PD method provides the fibre growth rates of up to 5 mm/min with the possibility of simultaneous pulling of several fibres [15]. Unlike the Czochralski process, μ-PD provides the growth of long single crystalline fibres in ready-to-use shape without a need of further cutting and polishing. Furthermore, μ-PD is a very efficient method for prompt screening of novel compositions.

Fabrication of inorganic scintillation materials in the form of fibres has a long history starting from the invention of the "Inverted Stepanov/EFG" methods in 1970s [16-18], and announcement of μ-PD method in Fukuda laboratory since the beginning of 1990s [19-23]. In recent years, the technologies of fibre growth have been continuously improved. One of the main issues is sustaining the uniform activator distribution in longitudinal and transverse directions of the fibre [24]. The melt from the crucible flows very fast to the crystallization area through the capillary. At a

CrystEngComm Accepted Manuscript

View Article Online
DOI: 10.1039/D1CE00091H

Published on 04 March 2021. Downloaded by Université Claude Bernard Lyon on 3/10/2021 9:05:29 AM.

relatively high pulling rate and absence of melt convection within the capillary, the admixture diffusion length is smaller than the capillary length, which is usually of 2-3 mm. Hence starting from a certain puling rate the longitudinal activator concentration is uniform as there is no diffusion of admixtures from the crystallization interface to bulk of the melt [25] in contrast Czochralski and other methods of bulk crystal growth. Meanwhile, admixtures are concentrated at the melt meniscus periphery and, then, captured by the growing fibre causing a substantial gradient of activator concentration in radial (transverse) direction and deterioration of light propagation along the fibre [26-29].

The μ-PD method was used for growing high melting point oxide scintillation crystals of $Lu_{2x}Y_{2-2x}SiO_5$:Ce (LYSO:Ce) [30], $Bi_4Ge_3O_{12}$ [31], $Lu_{2x}Gd_{2-2x}SiO_5$:Ce (LGSO:Ce) [32], and many more. Good radiation hardness and short radiation length of these materials make them promising for HEP experiments and other radiation detection applications. Meanwhile, in the crystals of solid solutions, such as LYSO:Ce and LGSO:Ce, the additional complications are caused by the segregation of larger host atoms (Y, Gd) to the periphery and SiO_2 evaporation. This result in melt non-stoichiometry owing to the composition shift in the equilibrium diagram [32]. These complications cause a low quality of silicate fibres owing to the mechanical stress and formation of parasite phases. For instance, $Lu_{2x}Gd_{2-2x}SiO_5$:Ce fibres at $x = 0.2$ and 0.5 and Ce concentrations 0.01 – 1.5 at.% were fabricated [32] following the optimal combination of scintillation parameters in them [33], relatively low melting temperatures [34]. The crystals with $x = 0.2$ demonstrated more cracks than those with $x = 0.5$ because of the vicinity of their compositions to polymorph transition in LGSO:Ce at $x = 0.17$ [34]. Meanwhile, following the X-ray diffraction of LGSO:Ce with the different Ce concentrations the fibres possessed the monoclinic C2/c structure and did not contain foreign phases.

The examples of halogenide fibre growth are not numerous. One should mention the growth of of $LaBr_3$:Ce, SrI_2:Eu, $CeCl_3$ fibres in Yoshikawa lab [35-37]. They were pulled down from a graphite crucible using a Pt seed. The developed method provided the growth of the hygroscopic halide materials without exposing them to ambient atmosphere at all stages starting from raw material preparation to unloading the grown crystal. The unstable melt meniscus did not allow obtaining good quality fibres with the length over few centimeters.

The largest progress has been achieved at growth of rare earth garnet fibres. LuAG:Ce is denser material with larger attenuation length for high energy particles, while YAG:Ce is lighter but

CrystEngComm Accepted Manuscript

View Article Online
DOI: 10.1039/D1CE00091H

Published on 04 March 2021. Downloaded by Université Claude Bernard Lyon on 3/10/2021 9:05:29 AM.

cheaper option keeping in mind the cost of Lu_2O_3 and Y_2O_3 raw materials. As YAG:Ce does not contain very heavy atoms, it should possess better radiation hardness under high energy hadrons compared to PWO and other heavy scintillators [38]. First reports on growth of garnet fibres by μ-PD are dated back to 2007 – 2009 [26-29]. By the analogy to Ce-doped silicates, the fibre quality may deteriorate because activator segregates to the fibre lateral surface due to the large difference of host and activator cation sizes [24]. Gas bubbles in fibres were frequently observed at some critical melt oversaturation with gases. The tendency to increasing gas bubbles quantity was observed at a high Ce concentration in the melt [24].

During recent decade, in particular, in the frame of H-2020 Intelum project [39], a large amount of experiments [40-42] was carried out with the aim to obtain long garnet fibres with a high light yield of at least 10000 phot/MeV, fast timing (decay time <40 ns), and good longitudinal transparency with the light attenuation length not less than 40 cm. In this paper we review recent achievements in μ-PD growth of long YAG- and LuAG-based fibres in Institute of Light and Matter (Lyon, France).

2. Experimental

Crystalline fibres were grown by the micro-pulling-down technique. The YAG- and LuAG-based fibres of different shape (round-shaped of 1-2 mm in diameter, as well as square-shaped of 2x2 mm^2 size) were grown using Ir crucibles and afterheaters in flowing Ar atmosphere. The length of the fibres was up to 60 cm, and usually 100% of the melt was crystallized into the fibres. The grown fibres were annealed at 1200 °C in air. For modification of optical and scintillation properties we applied different raw material compositions, pulling rates, dopant concentrations, as well as non-stoichiometric melts containing different amounts of Al_2O_3 excess. The seeds (Fig. 1) comprised Ce-doped and undoped fibres grown previously by the μ-PD, or rods cut from bulk crystals.

The ground parts crystals grown from tungsten crucibles were taken from ISMA NAS of Ukraine [44] and Crytur [45]. Mg codopant was added to the composition in the form of MgO (purity 99.95%) or $MgCO_3$ ("pure for analysis"). An Al_2O_3 powder (RSA le Rubis, 99.999% purity) was added to the raw material to form the aluminum excess in melt.

CrystEngComm Accepted Manuscript

View Article Online
DOI: 10.1039/D1CE00091H

Published on 04 March 2021. Downloaded by Université Claude Bernard Lyon on 3/10/2021 9:05:29 AM.

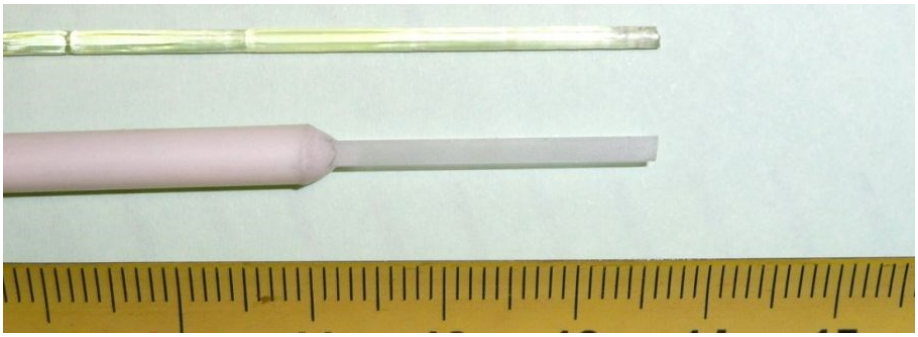

Fig. 1. LuAG:Ce seed [111] made of previously grown fibre (upper) and the seed of undoped LuAG [100] cut from the bulk crystal (lower).

To investigate the quantity of bubbles on the fibre surfaces and their longitudinal distribution, the optical binocular microscope LEICA DMR-XRE with two lighting sources and 50, 100, 200, 500, 1000) objective magnifications was used in transmission and reflection modes.

Attenuation length L_{att} (i.e., the fibre length where the intensity of LED-excited light falls by e times) was taken as the indicator of fibre optical quality. The attenuation length measurements were carried out using the custom made setup in CERN PH-CMX department under excitation with blue light in the 450-475 nm Ce^{3+} absorption band, see, for ex. [40] for details.

The light output of 10 mm long samples was measured under ^{137}Cs 662 keV γ-rays in CERN PH-CMX department. The integration gate was 1000 ns. Samples were wrapped with Teflon. Optical grease n~1.5 was used to couple one end of samples to PMT R2059. Quantum efficiency of PMT was about QE = 9.5 % for LuAG:Ce and QE = 7.0 % for YAG:Ce. Scintillation decay times were measured under the same type of excitation using an oscilloscope. The measurement details are described elsewhere [41].

3. Growth of long YAG:Ce and LuAG:Ce fibres

3.1. Design of the crucible and the capillary die

Control of melt meniscus shape and thickness is extremely important at growth of oxide fibers. Fiber cross section is determined by the crucible capillary die shape. Capillary dies can be made in a variety of shapes. Furthermore, it is possible to use a multi-capillary die to increase the production yield (Fig. 2). In the latter case, providing the uniform melt flow to the crystallization interface through all the dies is extremely difficult. Intensive research has been performed in ILM UMR 5306 CNRS (K. Lebbou team) in collaboration with ISMA (O. Sidletskiy team) regarding design and

CrystEngComm Accepted Manuscript

View Article Online
DOI: 10.1039/D1CE00091H

optimizations of this process can be found in numerous original papers [32, 40, 41, 42, 45-51]. In particular, Intelum H-2020 project has been a key factor in developing scintillating fibres design for HEP experiments.

Fig. 2. Multicapillary die crucible for simultaneous growing of three garnet fibres of a length up to 1.5 m and a diameter of 1 mm.

Despite the same crystalline structure and similar chemical composition and properties, crystallization conditions of yttrium and lutetium garnets are remarkably different. At first, a LuAG melt wettability is larger than that in YAG. The growth of fibre with a stable diameter is possible when melt wets just the bottom surface of the capillary die. The examples of a standard conical crucible and a crucible with elongated capillary die are shown in Fig. 3. A standard conical crucible (Fig. 3a) provides the stable growth of YAG fibres, while for LuAG the diameter control is complicated as melt wets the outer surface of the die (Fig. 3b). A modified crucible with the elongated capillary die possessing the wetting angle of 90° provided the growth of LuAG with a stable diameter.

Published on 04 March 2021. Downloaded by Université Claude Bernard Lyon on 3/10/2021 9:05:29 AM.
CrystEngComm Accepted Manuscript

View Article Online
DOI: 10.1039/D1CE00091H

Published on 04 March 2021. Downloaded by Université Claude Bernard Lyon on 3/10/2021 9:05:29 AM.

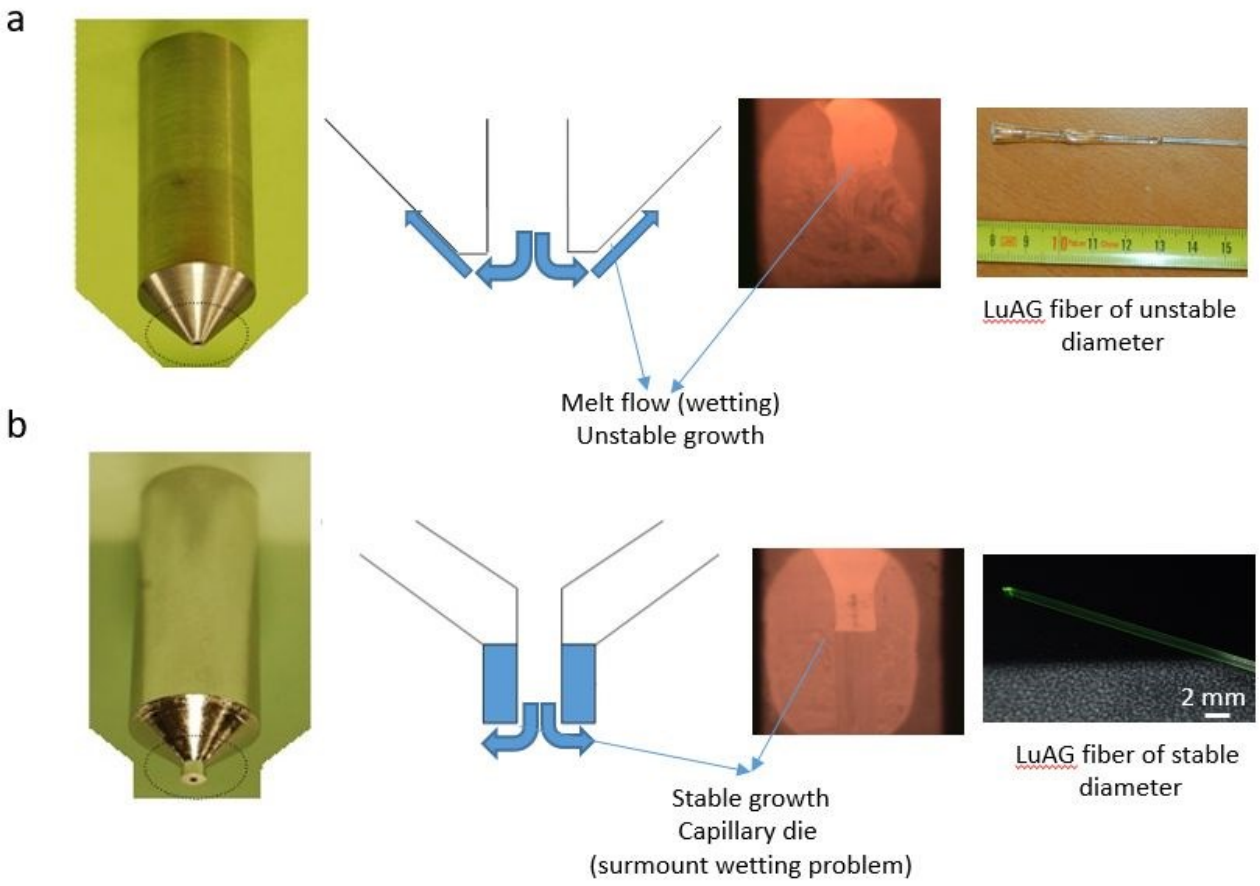

Fig. 3. (a) Ir crucible used for stable growth of YAG-based (a) and LuAG-based (b) crystalline fibers under stationary stable regime and (b) for fibres. Schematic representation of the flow directions of a highly wettable melt in the cases of standard conical crucible (a) and crucible with elongated capillary die (b) are shown in the right parts of the figures. The arrows indicate the melt flow directions.

3.2 Optimization of the raw material preparation procedure

Easy and reliable method of raw material preparation is necessary for large-scale production of scintillation fibres. Most of the growth experiments described in this paper were performed using cracked parts of crystals previously grown by the Czochralski method as a raw material. We have attempted to reduce the time and cost of the raw material preparation process by excluding the stage of Czochralski crystal growth. With this aim a series of LuAG fibres with a length of 20 cm and diameter of 1 mm were grown from crystalline raw materials, and powder raw materials prepared by the solid state reaction from oxides of the same purity.

CrystEngComm Accepted Manuscript

View Article Online
DOI: 10.1039/D1CE00091H

Published on 04 March 2021. Downloaded by Université Claude Bernard Lyon on 3/10/2021 9:05:29 AM.

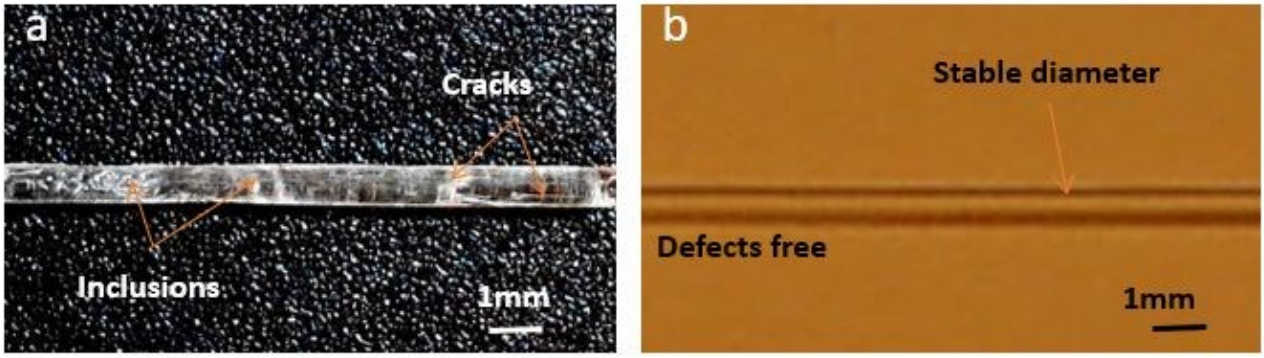

Fig. 4. LuAG fibres grown from the melt using sintered powders (a) and (b) crashed crystals as initial charge.

The stoichiometric ratio of Lu_2O_3 and Al_2O_3 was charged to the Ir crucible, and the solid-state reaction was performed right there to ensure the precise melt composition. The LuAG fibres produced from the powder synthesized by the solid-state reaction possessed remarkably worse transparency and rough surface (Fig. 4a). Better visible quality was achieved in the fibres grown from fragments of crystals obtained by the Czochralski method. All other growth conditions were kept the same. The latter fibre was homogeneous, with a smooth surface, and did not contain visible impurities (Fig. 4b). It was clearly shown that fibres grown from parts of previously grown crystals have certainly better shape and contain fewer defects compared to the fibres grown directly from powders. This evidently relates to:

1) smaller quantity of impurities in melt when using parts of Czochralski single crystals as the raw material, because the crystals are purified by recrystallization;

2) presence of foreign phase admixtures and local deviations from the stoichiometric composition occur in fibers when using unreacted powders as raw materials.

Therefore, all further experiments were performed using ground parts of YAG- and LuAG-based crystals as raw materials except the cases of Mg^{2+} doping and adding Al_2O_3 excess with powders.

3.3. Growth of LuAG and LuAG:Ce fibres

3.3.1. Effect of thermal gradient:

CrystEngComm Accepted Manuscript

View Article Online
DOI: 10.1039/D1CE00091H

Published on 04 March 2021. Downloaded by Université Claude Bernard Lyon on 3/10/2021 9:05:29 AM.

There is a tendency to the light attenuation length improvement through the thermal gradient control. The fibre growth rate is essentially controlled by the pulling rate. Steady growth conditions of fibre with a constant diameter are maintained if heat flow through the crystallization interface exactly balances the rate of latent heat release due to the crystallization process. Thermal conditions in the crystallizer significantly change during pulling of long fibres due to the heat sink through the elongating fibre. The delayed compensation of increased heat sink by power increasing results in meniscus overcooling and appearance of fibre diameter oscillations (Fig. 5).

Without the heat sink compensation, decrease of meniscus temperature moves the crystallization isotherm towards the crucible. As a sequence, melt inside the capillary die is partially or completely crystallized, thus, blocking melt supply to the meniscus [52]. As the issue, the melt does not wet the entire capillary die surface, and the diameters of the meniscus and the fibre decrease. However, the diameter decrease suppresses heat sink through the fibre, which in turn restores melt supply through the capillary. Such complication may be avoided by a heater power increase. Empirically we found that in the case of LuAG fibre the heat sink increase can be compensated by the gradual power increase by 0.12 % from the seeding stage till the end of a 25 cm long fibre growth process (Fig. 6). Meanwhile, during the growth of Ce doped fibres the power increase was 1.9 % relatively to the seeding stage. Obviously this significant difference is linked to larger radiant heat sink through LuAG:Ce fibres, as the latter show larger light attenuation length compared to LuAG [53]. Overall, the value of heater power correction can serve as an indicator of good fiber transparency: YAG:Ce and LuAG possess small light attenuation length in contrast of LuAG:Ce and LuAG:Pr.

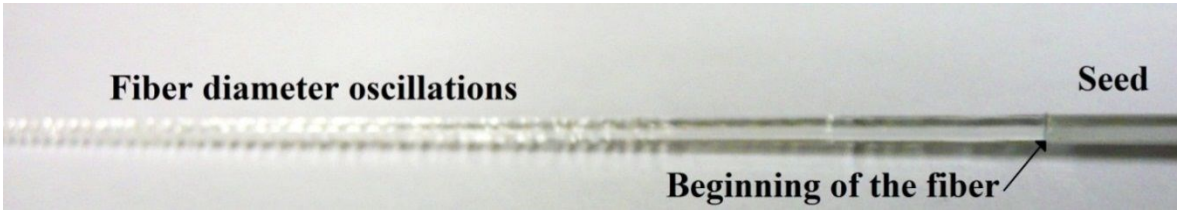

a

b

CrystEngComm Accepted Manuscript

View Article Online
DOI: 10.1039/D1CE00091H

c

Fig. 5. Parts of as-grown LuAG fibre: a) start of diameter oscillations in the beginning of growth; b) middle parts with the diameter oscillations; c) end of the fibre after the heater power correction.

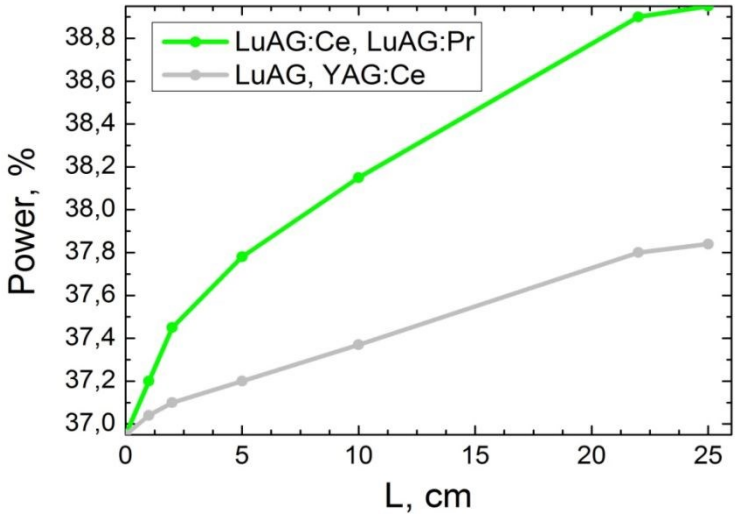

Fig. 6. Trends of heating power vs. fibre length.

3.3.2. Effect of growth rate.

Undoped and Ce-doped LuAG fibres with the length over 22 cm were grown at the pulling rates from 0.2 to 0.75 mm/min which were determined using a parametric approach [54]. The undoped fibers were colorless, while Ce-doped fibres were yellowish due to Ce^{3+} ion absorption. Fibers of both types were transparent, with a smooth surface, without visible macroscopic defects such as cracks and bubbles (Fig. 7). The Ce concentration in LuAG:Ce fibres ranged from 0.01 to 1.5 at.%. Any composition evolution resulting in a second-phase formation was not observed at the Ce^{3+} concentration of up to 0.1 at%. Disconnection of the fibre from the meniscus was never observed even in the case of sharp change of the pulling rate.

Published on 04 March 2021. Downloaded by Université Claude Bernard Lyon on 3/10/2021 9:05:29 AM.

CrystEngComm Accepted Manuscript

View Article Online
DOI: 10.1039/D1CE00091H

Published on 04 March 2021. Downloaded by Université Claude Bernard Lyon on 3/10/2021 9:05:29 AM.

Fig. 7. (a) Undoped LuAG and (b) Ce-doped LuAG fibers grown under the optimized conditions.

The optical microscopy observations indicated that the surface quality of LuAG fibres grown at pulling rates lower than 0.3 mm/min is better than the fibres grown at higher pulling rates (Fig. 8). The comparison of light attenuation and fiber surface quality evidences that a good surface quality is crucial to obtain reasonable light attenuation lengths (Fig. 9). Bubbles favor light scattering and escape through lateral faces. Therefore, the indicated pulling rate is essential to get LuAG fibres of a good optical quality.

CrystEngComm Accepted Manuscript

View Article Online
DOI: 10.1039/D1CE00091H

Published on 04 March 2021. Downloaded by Université Claude Bernard Lyon on 3/10/2021 9:05:29 AM.

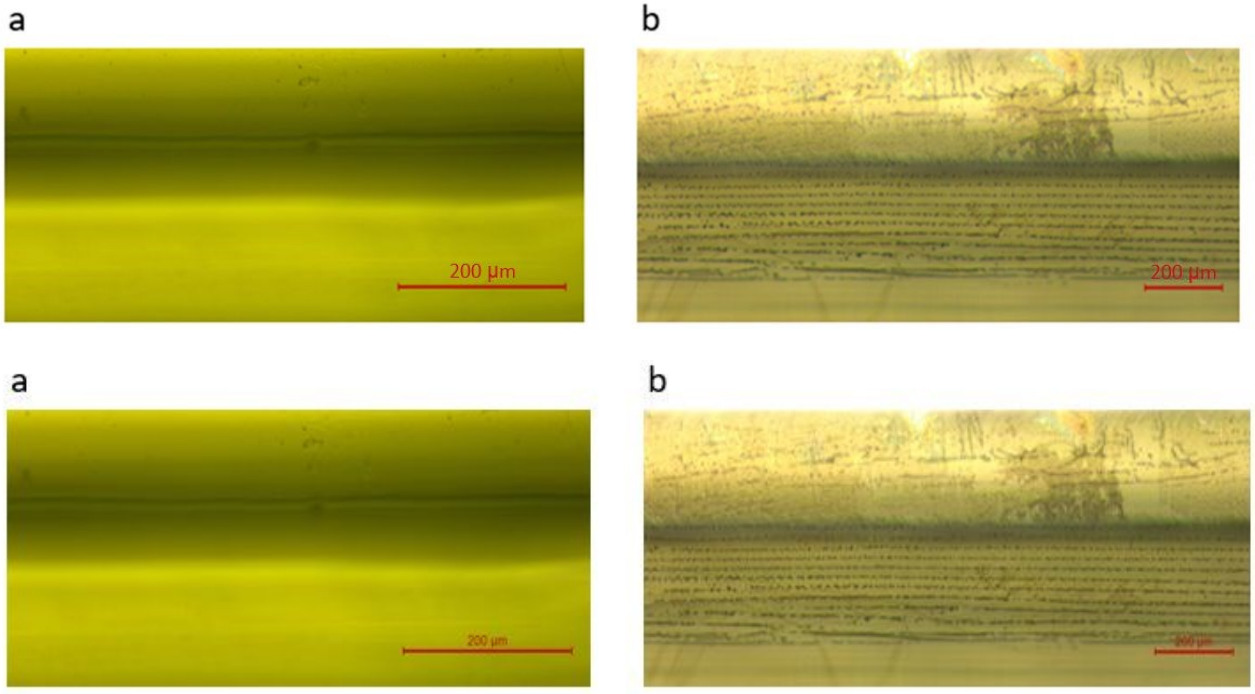

Fig. 8. Surface quality of LuAG fibres as a function of the pulling rate: (a) 0.3mm/min, (b) 0.5 mm/min.

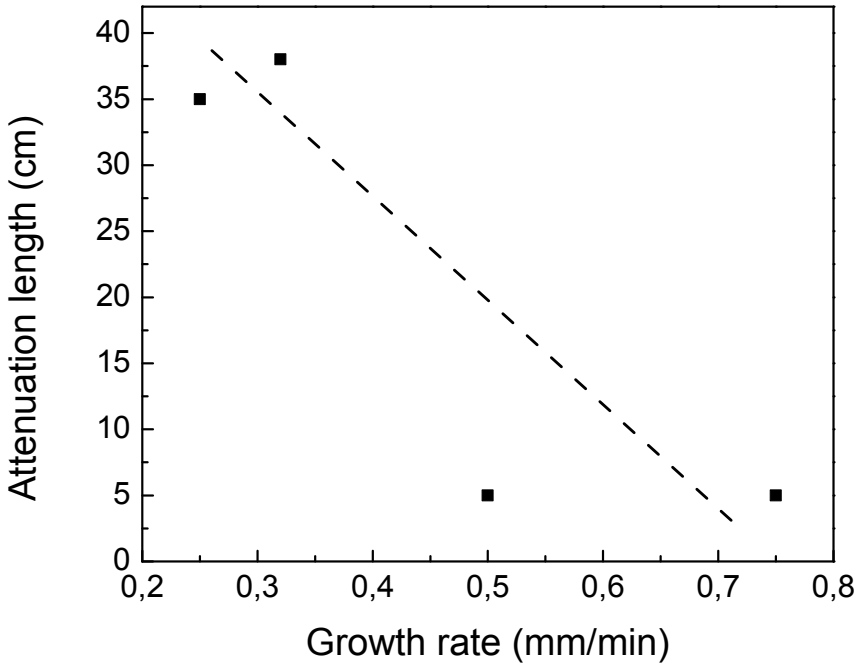

Fig. 9. Dependence of attenuation length on growth rate of LuAG fibres.

CrystEngComm Accepted Manuscript

View Article Online
DOI: 10.1039/D1CE00091H

Published on 04 March 2021. Downloaded by Université Claude Bernard Lyon on 3/10/2021 9:05:29 AM.

While no gas bubbles were observed in undoped LuAG crystals regardless of the pulling rates of up to 0.3 mm/min, strings of bubbles were observed along the growth direction in the fibres heavy doped with Ce (Fig. 10) and grown at the pulling rate of 0.5 mm/min. The presence of bubbles was certainly correlated with the Ce-doping, though the activator was introduced also in the form of crystalline LuAG:Ce. Usually such inclusions at crystal growth from the melt appear at some critical supersaturation of the melt with a gas impurity whose distribution coefficient is usually less than unity. The bubble segregation occurring during a liquid-solid transition leads to merging of the bubbles with subsequent buoyancy-driven floating up.

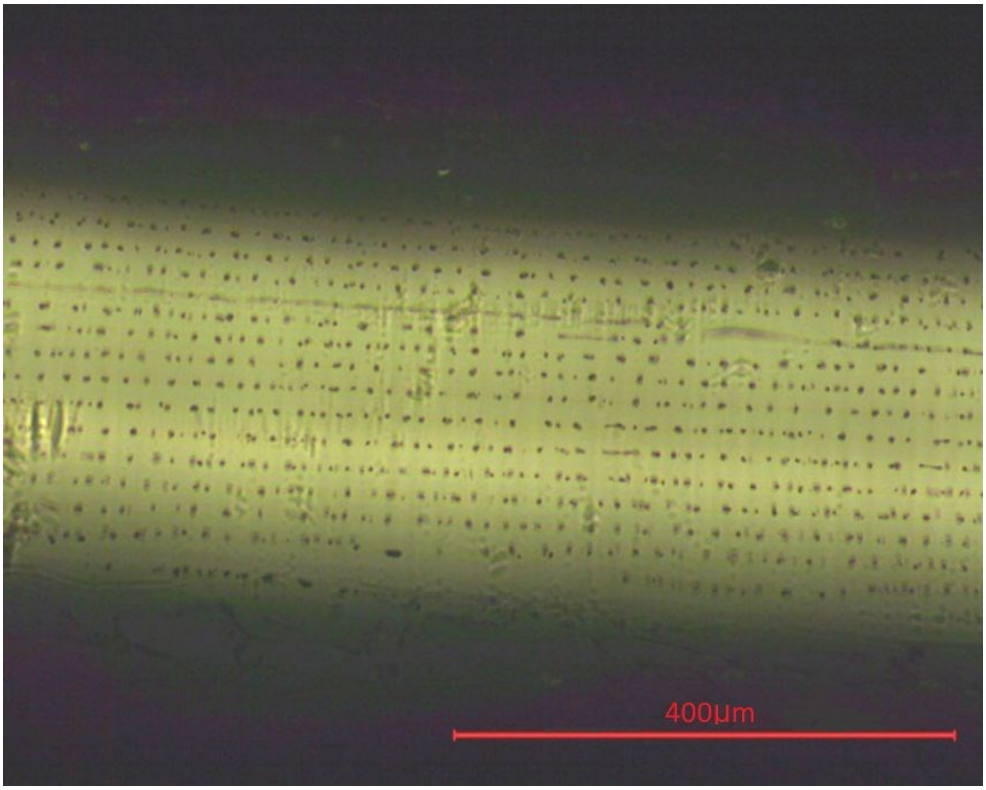

Figure 10. Bubbles inside LuAG:Ce fibre oriented along the growth axis.

Meanwhile, smaller size bubbles eventually diffused into fibers. Most of bubbles have a spherical geometry and some of them are elongated along the growth direction. A similar situation was observed when growing sapphire fibres using the same capillary channel [55]. Optical microscopy shows that bubbles were aligned well along the fibre axis (Figure 7). For the low pulling rates of 0.3 – 0.5 mm/min and low Ce concentration in the melt (<0.1 at%), the crystallization interface is flat and there is only one lateral layer of bubbles. The average periphery layer containing bubbles was

CrystEngComm Accepted Manuscript

View Article Online
DOI: 10.1039/D1CE00091H

Published on 04 March 2021. Downloaded by Université Claude Bernard Lyon on 3/10/2021 9:05:29 AM.

about 93 μm thick. The rest of the crystals volume was bubble free. The behavior was similar for the different parts of the fibres (beginning, middle and the end). These conditions ensure a low quantity of bubbles, which are only formed in the regions with minimum component of the melt velocity ahead solidification interface [52]. At velocity higher than the critical maximum growth rate, constitutional undercooling generates massive bubble incorporation.

3.3.3. Radial distribution of Ce^{3+}.

In the case of Ce-doped LuAG fibres, a substantial gradient of the Ce concentration might appear in the radial direction and have a negative impact on the fibre attenuation length. Cathodoluminescence microscopic imaging of the fibre cross section is an easy method to evaluate the activator distribution in the fibres (assuming the proportionality between the activator concentration and the emission intensity). Without codoping, Ce should be preferably is the trivalent state as it substitutes trivalent lanthanide cations. Remarkable quantity of Ce^{4+} was evidenced [56, 57] only in crystals codoped with divalent or monovalent cations where Ce^{4+} formation is favorable to compensate the excess negative charge introduced by the aliovalent substitution. Therefore, for LuAG:Ce and YAG:Ce we presume that Ce^{3+} and total Ce concentrations are equivalent.

In the cathodoluminescence experiments we used samples fabricated from LuAG:Ce fibres grown at different rates and with different Ce concentrations (Fig. 11). All the regions from which the samples were cut were ~1 cm distant from the beginning of the fibres. Following the brightness distribution at the photos the most of activator was concentrated at the fibre periphery (Fig. 12).. The radial Ce concentration showed a concave curvature for Ce-doped LuAG grown at 0.35 mm/min and nearly flat profile for Ce-doped LuAG grown at 0.5 mm/min, but slightly higher concentration in the periphery of the fibre, that is typical for activated garnets [58]. There are several ways to improve radial distribution of activator in fibre grown by μ-PD/EFG techniques, for example, simultaneous fiber growth from the crucibles with several capillaries [59], or increasing growth rate. But despite of improved radial activator distribution, overall optical quality deteriorates in fibres grown in such conditions.

CrystEngComm Accepted Manuscript

View Article Online
DOI: 10.1039/D1CE00091H

Published on 04 March 2021. Downloaded by Université Claude Bernard Lyon on 3/10/2021 9:05:29 AM.

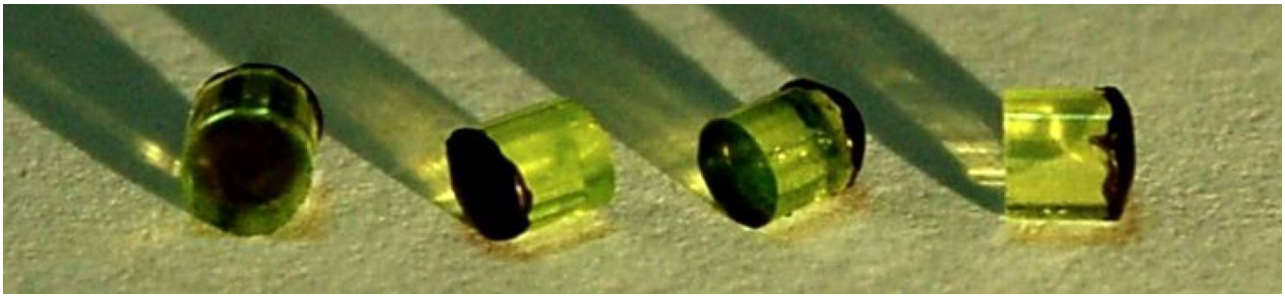

Fig.11. Samples of LuAG:Ce prepared for cathodoluminescence measurements (covered with black paint from one side).

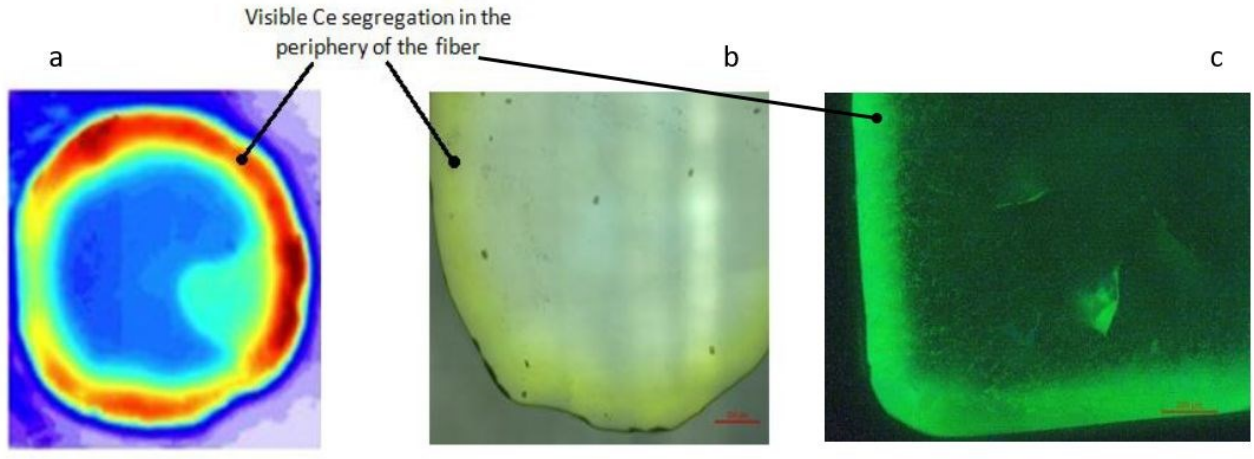

Fig. 12. Cerium segregation in LuAG:Ce fibre grown at a pulling rate of 0.25 mm/min: (a) cerium luminescence under X-ray excitation (red part corresponds to a high cerium concentration), (b) optical microscopy image illustrating cerium segregation in the periphery, (c) image at UV lamp excitation (365 nm) showing Ce segregation in the periphery.

By the analogy to LuAG:Ce, a qualitative radial distribution of activator (Ce^{3+}) in the grown fibres can be evaluated by brightness of microscopic images under UV-excitation. The tendency was similar to LuAG:Ce – more sharp segregation of Ce^{3+} to the surface was observed at higher Ce concentration in the melt.

3.4. Growth of YAG-based fibres

3.4.1. Growth from stoichiometric melt

CrystEngComm Accepted Manuscript

View Article Online
DOI: 10.1039/D1CE00091H

Published on 04 March 2021. Downloaded by Université Claude Bernard Lyon on 3/10/2021 9:05:29 AM.

Further efforts have been focused on YAG:Ce fibres as a low-cost alternative to LuAG:Ce because of cheaper raw materials. YAG–based fibres were grown using different raw materials and codopants to find the best property-quality combination. Mg-codoping was reported to decrease the scintillation decay time in YAG:Ce [51, 60]. Meanwhile, there are some issues connected with introducing Mg^{2+} codopant. As in YAG:Ce,Mg-codoped fibres Mg^{2+} was introduced to the melt in the powder form, this may be the main origin of scattering centers appearance in fibres. Furthermore, in the Mg^{2+}-codoped fibres, Mg^{2+} and Ce^{4+} radial distribution gradient may affect optical properties. The presence of cerium mainly in the tetravalent state at Mg^{2+}-codoping was certified by visual transparency of Mg^{2+}-containing fibre [41], because Ce^{4+} ions, unlike Ce^{3+}, do not possess absorption bands in the visible range. In our experiments, the concentrations of Ce and Mg codopants were varied within 100-1000 ppm and 25-120 at.ppm, respectively. Nevertheless, a similar activator distribution in YAG:Ce and in LuAG:Ce with the excellent attenuation length around 1.0 m did not result in a comparable attenuation length in YAG:Ce. Therefore, further we focused on effect of pulling rate on the fibre quality. The tendency to L_{att} decrease with increasing fibre growth rate in the 0.15-0.7 mm/min range was confirmed [41], while the addition of Mg resulted in further deterioration of attenuation length down to 3-16 cm.

3.4.2. Growth from non-stoichiometric melt

Apart of oxygen vacancies and antisites that are inherent to YAG/LuAG crystals, see, for example [61], we presumed that the degradation of fibre transparency may be attributed to the presence of Al^{3+} vacancies as reported in [62]. The depletion of melt and fibre surface with Al and oxygen ions is possible keeping in mind the melt overheating in μ-PD method, as well as flowing Ar gas atmosphere, though no deposit on the crystallizer walls, or other evidence of Al_2O_3 evaporation due to decomposition into volatile Al_2O and O_2 was observed. Meanwhile, strong depletion of Czochralski grown YAG crystal surface was reported by us in [63]. Therefore, we have focused on YAG-based fibres grown from the non-stoichiometric melt with the Al_2O_3 excess, which may eventually compensate the losses due to evaporation.

The concentration of Ce in the melt varied within the 100-200 ppm range, the magnesium concentration was up to 40 ppm. The fibres were grown with the rates of 0.2-0.3 mm/min. The lengths of grown fibres were 25 – 55 cm. Then the fibres were cut into the 22 cm long samples (for attenuation length measurement) and ~1 cm long samples for scintillation decay time measurements.

CrystEngComm Accepted Manuscript

View Article Online
DOI: 10.1039/D1CE00091H

Published on 04 March 2021. Downloaded by Université Claude Bernard Lyon on 3/10/2021 9:05:29 AM.

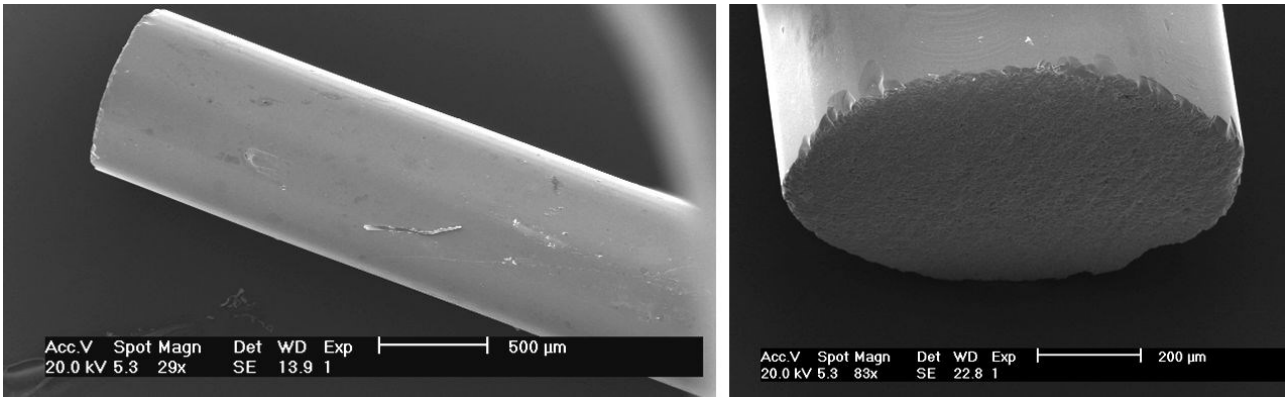

Fig. 13. Longitudinal and transversal sections of YAG:Ce fibre.

To evaluate the effect of Al excess, a series of YAG:Ce fibres (Table 1) was produced with the Al^{3+} excess of 20 – 370 ppm in the melt compared to the $3Y_2O_3{:}5Al_2O_3$ stoichiometric composition. A typical fibre consisted of the transparent part (closer to the seed) and opaque part with a very low light transmission [42]. While overall L_{att} in 22 cm long fibres deteriorated with Al^{3+} excess introduction, the the L_{att} in the head parts was improved from 16.5 to up to 20-27 cm.

Table 1. Attenuation length in YAG:Ce fibres grown from melt with different Al^{3+} excess.

Al excess, ppm	Overall L_{att}, cm	L_{att} of the transparent part, cm	Length of the transparent part, cm
<20	17.4	16.5	22
110	14.4	20.0	16
160	16.3	20.3	18
210	10.4	26.7	15
370	6.0	21.8	11

Electron Probe micro-analysis (EPMA) of the fibres containing small and large Al excess showed that cerium segregates to the fibre tail at the heavy Al^{3+} excess of high 370 ppm, and the X-ray diffraction (XRD) showed that opaque part contains Al_2O_3 phase inclusions [42]. This means that adding Al_2O_3 excess into the melt compensates the Al^{3+} deficiency in the beginning of fibres, whereas its accumulation in the melt at further growth stages leads to formation of Al_2O_3 phase

CrystEngComm Accepted Manuscript

View Article Online
DOI: 10.1039/D1CE00091H

inclusions in the opaque parts of the fibres. The largest L_{att} of 26.7 cm is achieved at 210 ppm excess of Al^{3+}, but the transparent part length decreases down to 15 cm. Therefore, the Al excess should not exceed approximately 200 ppm to grow a 22 cm long fibres with a good transparency.

Published on 04 March 2021. Downloaded by Université Claude Bernard Lyon on 3/10/2021 9:05:29 AM.

3.4.3. Improving stability of crystallization conditions of long fibres

In parallel we worked on enhancing the stability of crystallization conditions assuming the melt meniscus instability in the end of growth may be an important factor of fibre quality degradation. By controlling the thermal conditions the fibres were crystallized from the ca. 0.1 - 0.5 mm thick melt meniscus. The meniscus thickness of 0.1 – 0.2 mm was considered as optimal, while with fibre elongation and increase of heat removal through the fibre, the meniscus thickness tended to decrease below 0.1 mm, and the meniscus thickness over 0.2 mm resulted in a high sensitivity of growth process to external vibrations. In meniscus with the thickness less than 0.1 mm the melt convection is weak, and admixtures segregated by the crystallization interface tend to accumulate in the periphery of the fibre. Additionally, there is a danger of fibre contact with the capillary die resulting in fibre shape deterioration (see section 3.3.1). Therefore, we attempted to maintain the stable meniscus thickness of 0.1 – 0.2 mm.

Under the stable heating power the meniscus thickness is determined by the two basic factors: vertical thermal gradient at the crystallization interface, and melt pressure inside the capillary die.

The 1.5 times difference in LuAG and YAG densities (6.73 vs. 4.55 g/cm^3) affects the crystallization conditions, especially when a small amount of melt is loaded into the crucible. At small column height of light YAG melt, the pressure in capillary die may be not enough for wetting of the capillary bottom surface. In this case, the growth is unstable with high amount of inclusions in fibres. Therefore, the pressure in the capillary was increased by filling the crucible with larger amount of initial raw material. This provided us with the fibres with the length of up to 55 cm.

CrystEngComm Accepted Manuscript

View Article Online
DOI: 10.1039/D1CE00091H

Published on 04 March 2021. Downloaded by Université Claude Bernard Lyon on 3/10/2021 9:05:29 AM.

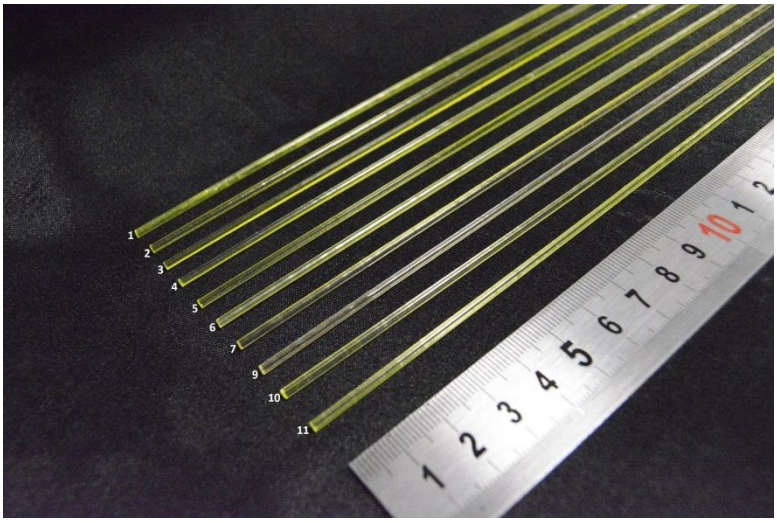

Fig. 14. Photo of a series of YAG fibres grown under stationary conditions.

Following the results obtained with the 25 cm long fibres, Al^{3+} excess in the 0-220 ppm range was introduced into the melt to adjust the optimal Al^{3+} concentration in 55 cm long fibres. The fibres cut from the head parts were visually more transparent whereas the fibres cut from tail parts contained visible inclusions. The L_{att} in the 22 cm long fibres increased up to 36 cm. The optimal Al excess in such fibres grown under the optimized thermal conditions is approximately 120 ppm [42].

Table 2. Attenuation length and scintillation decay time in YAG:Ce,Mg,Al fibres.

$C(Al_{doped})$, Ppm	C(Mg), Ppm	Attenuation length, cm	Decay times, ns
0	0	17.6	129
0	20	24.3	108
0	40	35.7	80
170	0	30.4	142
170	20	6.2	97
170	40	4.2	86

3.4.4. Effect of Mg codoping on scintillation decay time

Co-doping with Mg reduced the scintillation decay times of both fast and slow components, and increased the fast component contribution into the overall signal [42]. The shortest decay time of 80

CrystEngComm Accepted Manuscript

View Article Online
DOI: 10.1039/D1CE00091H

Published on 04 March 2021. Downloaded by Université Claude Bernard Lyon on 3/10/2021 9:05:29 AM.

ns was observed at 40 ppm Mg codoping. The decay times clearly decrease with Mg concentration (Table 2) pointing that further increasing of Mg concentration above 40 ppm is necessary to reduce the decay time to 40 ns as requested. The decay times do not correlate with the absence/presence of Al excess, whereas Mg-codoped fibres should be grown without Al excess addition, as it sharply reduces the fibre attenuation length (see Table 2). As the decay time below 40 ns was achieved in LuAG:Ce,Mg with heavy Mg doping with the ratio of $1Ce^{3+}$:$3Mg^{2+}$, there is a room for heavier Mg doping of YAG:Ce,Mg fibres.

4. Post-growth annealing of LuAG- and YAG-based fibres

The effect of annealing was checked with fibres grown under two types of inert argon atmospheres with different oxygen admixture concentrations (Table 3). The fibres grown with different pulling rates and crystallographic orientations were annealed during 24 hours in air atmosphere at 1200°C. Post-growth annealing of oxide crystals in oxidizing or inert atmosphere usually contributes to improvement of their transparency [64]. In rare-earth garnets, the annealing may suppress color centers formed at electron capture by oxygen vacancies, or oxygen vacancy related complex defects [63]. However, this effect was negligible for the YAG:Ce fibres.

Antisite defects, namely Y or Lu occupied Al^{3+} sites are the most probable defects in garnets following the very low formation energies in accordance with ab-initio calculations [65]. Different point defects, such as oxygen vacancies are tend to form near antisites. These defects act as electron traps forming color centers, which deteriorate crystal transmission. The probability of antisite formation increases when the difference in ionic radii between Al^{3+} and substitutional cation is small. Therefore, substitution of Al^{3+} with smaller Lu^{3+} is more probable than that with larger Y^{3+}, hence more antisites should form in LuAG. This describes no annealing effect on YAG:Ce attenuation length. Assuming that less antisites are formed in as-grown YAG than those in LuAG due to larger ionic radii difference between Y^{3+} and Al^{3+}, this describes no annealing effect on YAG:Ce attenuation length. In YAG:Ce,Mg fibres, L_{att} increased by up to 4 times, but the absolute values were still very low – up to 13 cm.

On the other hand, the attenuation length of Ce-doped LuAG was significantly improved, especially for fibres grown with the 0.3 mm/min rate. The largest attenuation length of more than 1 meter was achieved in LuAG:Ce fibres grown along [100] direction [40].This value is by a factor of 2 larger than that in the fibre grown along [111]. This is a strong indication that annealing the grown fibre significantly improves the attenuation length of Ce-doped LuAG fibres grown at low pulling

CrystEngComm Accepted Manuscript

View Article Online
DOI: 10.1039/D1CE00091H

Published on 04 March 2021. Downloaded by Université Claude Bernard Lyon on 3/10/2021 9:05:29 AM.

rates. In addition, these results show that annealing does not strongly improve the attenuation of the fibres grown at 0.5 mm/min and, consequently, pulling rate remains as the most important factor. Thus, the high pulling rate may introduce new intrinsic defects, or remarkably change a concentration of the mentioned defects. In addition new defects may be created which need high temperature and long time to be eliminated. However, we no structural changes and no visible change in fiber coloration were detected. A deeper optical study is necessary to clarify the mechanism of transparency improvement by the annealing.

Table 3. Effect of annealing on attenuation length of YAG:Ce and and LuAG:Ce fibres.

Sample	Orientation	Growth rate, mm/min	Ce conc, ppm	Attenuation length, cm	
				as-grown	annealed
YAG:Ce	111	0.2	150	10	10
YAG:Ce	111	0.2	150	18	18
LuAG:Ce	100	0.3	100	13	104
LuAG:Ce	111	0.3	100	17	50
LuAG:Ce	100	0.5	100	13	14
LuAG:Ce	111	0.5	100	18	23

One should not rule out that the Lu or Y substitution by Ce into the crystal structure of LuAG and YAG introduces distortion due to the different radii of dopant and host ions. Independently on the shape of the crystals, such distortions in Ce-doped LuAG crystals will create mechanical stress during cooling, and this is a major source of dislocation in as grown fibres. The formed microscopic defects can be the reason of observed bad light propagation in some of the grown fibres.

Therefore, the annealing of the fibres significantly improves the attenuation length of Ce-doped LuAG fibres and can be attributed to the elimination of color centers responsible for carrier trapping, whereas annealing of YAG:Ce under the same conditions have not provided a remarkable positive effect.

5. Summary

CrystEngComm Accepted Manuscript

View Article Online
DOI: 10.1039/D1CE00091H

Published on 04 March 2021. Downloaded by Université Claude Bernard Lyon on 3/10/2021 9:05:29 AM.

The development of shaped μ-PD crystal growth was a great technological advance provided us with high-quality single crystalline fibres of rare earth garnet. The feasibility of mass production of LuAG and LuAG:Ce fibres with the lengths over 22 cm was demonstrated. The growth process was optimized to obtain undoped and Ce-doped LuAG fibres with enhanced attenuation lengths over 22 cm and without micro- and macroscopic defects such as cracks, inclusions.

The optimal growth conditions of LuAG and LuAG:Ce growth were determined:

- Ground single crystals as raw material;
- Custom crucible design;
- Growth rate of 0.3 mm/min;
- Ce concentration – less than 0.05 at. %;
- No reproducible effect of crystal orientation on quality of LuAG and LuAG:Ce was noticed,
- post growth thermal annealing in air (24 h);
- Increasing the heating power by 0.12 % for undoped and by 1.9 % in 22 cm long Ce-doped fibres is necessary to provide stable thermal conditions during the process.

It was revealed that LuAG:Ce fibre growth technology has to be modified to obtain YAG:Ce of comparable quality. The significant progress in transmission of YAG:Ce-based fibres has been achieved by adding of Al^{3+} excess into the melt and optimizing thermal conditions of crystallization. by increasing thermal gradient, and rising melt pressure in the capillary die by adding more raw material into the crucible. As the result, the attenuation length of up to 38 cm was achieved in 22 cm long YAG:Ce fibres. The Mg-codoped fibres did not show the tendency to L_{att} improvement with adding Al^{3+} excess. However, optimization of thermal conditions and post-growth annealing provided the attenuation length enhancement up to 36 cm in YAG:Ce,Mg, while the scintillation decay time of 80 ns is still too slow for the HEP applications.

The optimal growth conditions of YAG and YAG:Ce growth were the follows:

- growth rate of 0.3 mm/min;
- Ce concentration of up to 0.1 at%;
- Al excess in melt - 100-200 ppm (for Mg-free YAG:Ce);
- Mg concentration over 40 ppm;
- post growth thermal annealing in air (24 h);
- increasing the heating power by 0.85 % for undoped YAG and 2,4% for doped YAG:Ce (55 cm long) is necessary to provide stable thermal conditions during the process.

CrystEngComm Accepted Manuscript

View Article Online
DOI: 10.1039/D1CE00091H

Published on 04 March 2021. Downloaded by Université Claude Bernard Lyon on 3/10/2021 9:05:29 AM.

Acknowledgements

The work is partially supported by the Marie Skłodowska-Curie Research, Innovation Staff Exchange Project H2020-MSCA-RISE-2014 no.644260 "INTELUM" and is made in the frame of Crystal Clear Collaboration in CERN. Also we acknowledge the support from the International Research Project "ScintLab" of National Center for Scientific Research (CNRS) of France.

References

1. V. A. Batarin, J. Butler, T. Y. Chen, A. M. Davidenko, A. A. Derevschikov, Y. M. Goncharenko, V. N. Grishin, V. A. Kachanov, V. Y. Khodyrev, A. S. Konstantinov, V. I. Kravtsov, Y. Kubota, V. S. Lukanin, Y. A. Matulenko, Y. M. Melnick, A. P. Meschanin, N. E. Mikhalin, N. G. Minaev, V. V. Mochalov, D. A. Morozov, L. V. Nogach, A. V. Ryazantsev, P. A. Semenov, V. K. Semenov, K. E. Shestermanov, L. F. Soloviev, S. Stone, A. V. Uzunian, A. N. Vasiliev, A. E. Yakutin, J. Yarb, *Nucl. Instrum. Methods Phys. Res., A*, 2004, **530**, 286-292.
2. J. Coupard, H. Damerau, A. Funken, R. Garoby, S. Gilardoni, B. Goddard, K. Hanke, A. Lombardi, D. Manglunki, M. Meddahi, B. Mikulec, G. Rumolo, E. Shaposhnikova, M. Vretenar (eds.), LHC Injectors Upgrade. Technical Design Report**,** 2014.
3. G. Mavromanolakis, E. Auffray, P. Lecoq, *J. Instrum.*, 2011, **6**, 10012.
4. The Linear Collider Collaboration and the global ILC community, The International Linear Collider. A Global Project, 2019.
5. M. Lucchini, T. Medvedeva, K. Pauwels, C. Tully, A. Heering, C. Dujardin, K. Lebbou, P. Lecoq, E. Auffray, *J. Instrum.*, 2013, **8,** P10017–P10017.
6. P. Lecoq, *J. Phys. Conf. Ser.,* 2009, **160**, 012016.
7. C. Dujardin, C. Mancini, D. Amans, G. Ledoux, D. Abler, E. Auffray, P. Lecoq, D. Perrodin, A. Petrosyan, K. L. Ovanesyan, *J. Appl. Phys*, 2010, **108**, 013510.
8. K. Pauwels, C. Dujardin, Gundacker, K. Lebbou, P. Lecoq, M. Lucchini, F. Moretti, A. G. Petrosyan, X. Xub, E. Auffraya, *J. Instrum.*, 2013, **8**, 09019.
9. X. Xu, K. Lebbou, F. Moretti, K. Pauwels, P. Lecoq, E. Auffray, C. Dujardin, *Acta Mater.*, 2014, **67**, 232-238.

CrystEngComm Accepted Manuscript

View Article Online
DOI: 10.1039/D1CE00091H

Published on 04 March 2021. Downloaded by Université Claude Bernard Lyon on 3/10/2021 9:05:29 AM.

10. Benaglia, M. Lucchini, K. Pauwels, C. Tully, T. Medvedeva, A. Heering, C. Dujardin, V. Kononets, K. Lebbou, N. Aubry, S. Fara, G. Ferro, P. Lecoqa, E. Auffraya, *J. Instrum.*, 2016, **11**, 5004.

11. K. Kamada, R. Murakami, V. V. Kochurikhin, G. Luidmila, K. Jin Kim, Y. Shoji, A. Yamaji, S. Kurosawa, Y. Ohashi, Y. Yokota, A. Yoshikawa, *J. Cryst. Growth*, 2018, **492**, 45-49.

12. A. Nehari, A. Laidoune, M. Khetib, L. Grosvalet, A. Brenier, G. Panczer, G. Godfroy, S. Labor, K. Lebbou, *Opt. Mater.*, 2011, **34**, 365–367.

13. O. Benamara, K. Lebbou*, J. Cryst. Growth*, 2016, **449**, 67–74.

14. O. Sidletskiy, P. Arhipov, S. Tkachenko, Ia. Gerasymov, D. Kurtsev, V. Jarý, R. Kuˇcerková, M. Nikl, K. Lebbou, E. Auffray, *Springer Proc. Phys.*, 2019, **227**, 83-95.

15. Y. Yokota, V. Chani, M. Sato, K. Tota, K. Onodera, T. Yanagida, A. Yoshikawa, *J. Cryst. Growth*, 2011, **318**, 983–986.

16. K.M. Kim, G.W. Cullen, S. Berkman, A.E. Bell, Quarterly Progress Report No. 1, 1976, (ERDA/JPL/ 954465 -76/1, June).

17. Y. Mimura, Y. Okamura, Y. Komazawa, *J. Appl. Phys*., 1980, **19**, 269.

18. A.V. Stepanov, *The Future of Metalworking*, 1963, Lenizdat, Leningrad (in Russian).

19. D.H. Yoon, I. Yoninga, T. Fukuda, N. Ohnishi, *J. Cryst. Growth*, 1994, **142**, 339.

20. V.I. Chani, K. Nagata, T. Kawaguchi, M. Imaeda, T. Fukuda, *J. Cryst. Growth*, 1994, **194**, 374.

21. D.H. Yoon, T. Fukuda, *J. Cryst. Growth*, 1994, **144**, 201.

22. T. Fukuda, V. Chani, *Springer Adv. Mat. Res.*, 2007, **8**, 341.

23. T. Fukuda, P. Rudolph, *Cryst. Res. Tech.*, 1999, **34**, 3-40.

24. K. Lebbou, *Opt. Mater.*, 2017, **63**. 13-18.

25. A. Nehari, T. Duffar, E. A. Ghezal, K. Lebbou, *Cryst. Growth Des.* 2014, **14**, 12, 6492-6496;

26. Xu, X., Lebbou, K., Moretti, F., Pauwels, K., Lecoq, P., Auffray, E., & Dujardin, C., *Acta Mater.*, 2014, **67**, 232–238.

27. D. Sangla, N. Aubry, A. Nehari, A. Brenier, O. Tillement, K. Lebbou, F. Balembois, P. Georges, D. Perrodin, J. Didierjean, J. M. Fourmigue, *J. Cryst. Growth*, 2009, **312**, 125-130.

28. R. Simura, A. Yoshikawa, *J. Cryst. Growth*, 2009, **311**, 4763-4769.

29. D. Maier, D. Rhede, R. Bertram, D. Klimm, R. Fornari, *Opt. Mater.*, 2007, **30**, 11-14.

30. B. Hautefeuille, K. Lebboua, C. Dujardin, J.M. Fourmigue, L. Grosvalet, O. Tillement, C. Pedrini, *J. Cryst. Growth*, 2006, **289**, 172-177.

CrystEngComm Accepted Manuscript

View Article Online
DOI: 10.1039/D1CE00091H

Published on 04 March 2021. Downloaded by Université Claude Bernard Lyon on 3/10/2021 9:05:29 AM.

31. V. Chani, K. Lebbou, B. Hautefeuille, O. Tillement, J. M. Fourmigue, *Cryst. Res. Tech.*, 2006, **41(10)**, 972-978.

32. V. Kononets, O. Benamara, G. Patton, C.Dujardin, S. Gridin, A. Belsky, D. Dobrovolskas, A. Vaitkevičius, G. Tamulaitis, V. Baumer, K. Belikov, O. Sidletskiy, K. Lebbou, *J. Cryst. Growth*, 2015, **412**. 95–102.

33. O.Sidletskiy, A. Belsky, A. Gektin, S. Neicheva, D. Kurtsev, V. Kononets, C. Dujardin, K. Lebbou, O. Zelenskaya, V. Tarasov, K. Belikov, and B. Grinyov, *Cryst. Growth Des.*, 2012, **12**, 4411−4416.

34. M. Glowacki, G. Dominiak-Dzik, W. Ryba-Romanowski, R. Lisiecki, A. Strzep, T. Runka, M. Drozdowski, V. Domukhovski, R. Diduszko, M. Berkowski, *J. Solid State Chem.*, 2012, **186**, 268-277.

35. Y. Yokota, K. Nishimoto, S. Kurosawa, D. Totsuka, A. Yoshikawa, *J. Cryst. Growth*, 2013, **375**, 49-52.

36. Y. Yokota, S. Kurosawa, Y. Shoji, Y. Ohashi, K. Kamada, A. Yoshikawa, *Opt. Mater.*, 2017, **65**, 46-51.

37. R. Král, V. Jarý; J. Pejchal; S. Kurosawa, K. Nitsch, Y. Yokota, M. Nikl; A. Yoshikawa, *IEEE Trans. Nucl. Sci.*,2016, **63**, 453-458.

38. M. Korjik, *J. Instrum.*, 2017, **12**, 8021–80215.

39. http://intelum.web.cern.ch/

40. V. Kononets, E. Auffray, C.Dujardin, S.Gridin, F. Moretti, G. Patton, K. Pauwels, O. Sidletskiy, X. Xu, K. Lebbou, *J. Cryst. Growth*, 2016, **435**, 31–36.

41. V. Kononets, K. Lebbou, O. Sidletskiy, Yu. Zorenko, M. Lucchini, K. Pauwels, and E. Auffray, *Springer Proc. Phys.*, 2017, **200**, 114–128.

42. O. Sidletskiy, K. Lebbou, D. Kofanov, V. Kononets, I. Gerasymov, R. Bouaita, V. Jary , R. Kucerkova , M. Nikl , A. Polesel, K. Pauwels, E. Auffray, *CrystEngComm*, 2019, **21**, 1728-1733.

43. P. Arhipov, S. Tkachenko, S. Vasiukov, K. Hubenko, I. Gerasymov, V. Baumer, O. Sidletskiy, *J. Cryst. Growth*, 2016, **449**, 104–107.

44. www.cyberstar.fr

45. M. V. Derdzyan, K. L. Ovanesyan, A. G. Petrosyan, A. Belsky, C. Dujardin, C. Pedrini, E. Auffray, P. Lecoq, M. Lucchini, K. Pauwels, *J. Cryst. Growth,* 2012, **361**, 212-216.

CrystEngComm Accepted Manuscript

View Article Online
DOI: 10.1039/D1CE00091H

Published on 04 March 2021. Downloaded by Université Claude Bernard Lyon on 3/10/2021 9:05:29 AM.

46. T. S. Koroleva, M. M. Kidibaev, A. Nehari, C. Pedrini, K. Lebbou, A. N. Belsky, A. N. Tcherepanov, A. V. Ishchenko, V. Yu. Ivanov, I. N. Sedunova, O. S. Teslenko, L. V. Viktorov, B. V. Shulgin, L .H. Zheng, J. Xu, V. Kononets, O. Sidletskiy, *Opt. Mater.*., 2013, **35**, 868-874.

47. K. Pauwels, C. Dujardin, S. Gundacker, K. Lebbou, P. Lecoq, M. Lucchini, F. Moretti, A. G. Petrosya, X. Xu, E. Auffray, *JINST*, 2013 **8,** 1-17.

48. V. Kononets, D. Dobrovolskas, S. Neicheva, M. Starzhinsky, O. Sidletskiy, K. Lebbou, G. Tamulaitis*, IEEE Trans. Nucl. Sci.*, 2014, **61**, 343-347.

49. P. Arhipov, S. Tkachenko, Ia. Gerasymov, O. Sidletskiy, K. Hubenko, S. Vasyukov, N. Shiran, V. Baumer, P. Mateychenko, A. Fedorchenko, Y. Zorenko, Ya. Zhydachevskii, Kh. Lebbou, M. Korjik, , *J. Cryst. Growth*, 2015, **430**, 116–121.

50. A. Djebli, F. Boudjada, K. Pauwels, V. Kononets, G. Patton, A. Benaglia, M. Lucchini, F. Moretti, O. Sidletskiy, C. Dujardin, P. Lecoq, E. Auffray, K. Lebbou, *Opt. Mater.,* 2017, **65**, 66-68.

51. A. Belsky, K. Lebbou, V. Kononets, O. Sidletskiy, A. Gektin, E. Auffray, D. Spassky, A. N. Vasil'ev. *Opt. Mater.*, 2019, **92**, 341–346.

52. S. Wenjia, T. Duffar, A. Nehari, V. Kononets, K. Lebbou, , *J. Cryst. Growth*, 2017, **474**, 43–49.

53. Croissance cristalline de cristaux scintillateurs de LGSO et de grenats à partir de l'état liquide par les techniques Czochralski (Cz) et micro-pulling down (μ-PD) et leurs caractérisations, V. Kononets, L`universite Claude Bernard Lyon 1, 2014.

54. P. Rudolph, T. Fukuda, *Cryst. Res. Tech.,* 1999, **34**, 3–40.

55. E. A. Ghezal, H. Li, A. Nehari, G. Alombert-Goget, A. Brenier, K. Lebbou, M. F. Joubert, M. T. Soltani, *Cryst. Growth Des.*, 2012, **12**, 4098–4103.

56. Y. Wu, F. Meng, Q. Li, M. Koschan, C. L. Melcher, *Phys. Rev. Appl.*, 2014, **2**, 044009.

57. G. Dantelle, G. Boulon , Y. Guyot, D. Testemale, M. Guzik, S. Kurosawa, K. Kamada, A. Yoshikawa, *Phys. Status Solidi B*, 2020, **257**, 1900510.

58. K. Lebbou, D. Perrodin, V. I. Chani, A. Brenier, O. Tillement, *J. Am. Ceram.*, 2006, **89**, 75–80.

59. Y. Yokota, T. Kudo, V. Chani, Y. Ohashi, S. Kurosawa, K. Kamada, Z. Zengd , Y. Kawazoe A. Yoshikawa, *J. Cryst. Growth*, 2017, **474**, 178–182.

60. M. Nikl, K. Kamada, V. Babin, J. Pejchal, K. Pilarova, E. Mihokova, A. Beitlerova, K. Bartosiewicz, S. Kurosawa, Akira Yoshikawa, *Cryst. Growth Des.*, 2014, **14**, 4827−4833.

CrystEngComm Accepted Manuscript

View Article Online
DOI: 10.1039/D1CE00091H

61. V. Laguta, M.Buryi, P. Arhipov, O. Sidletskiy, O. Laguta, M. G. Brik, M. Nikl, *Phys. Rev. B,* 2020, **101**, 024106.

62. F. Selim, D. Winarski, C. Varney, M.C. Tarun, J. Ji, M.D. McCluskey, *Res. Phys.*, 2015, **5**, 28-31.

63. S. Tkachenko, P. Arhipov, I. Gerasymov, D. Kurtsev, S. Vasyukov, V. Nesterkina, N. Shiran, P. Mateichenko, O. Sidletskiy, , *J. Cryst. Growth*, 2018, **483**, 195–199.

64. K. Brylew, W. Drozdowski, M. E. Witkowski, K. Kamada, T. Yanagida, A. Yoshikawa, *Cent. Eur. J. Phys.*, 2012, **11,** 138-142.

65. C. R. Stanek, K. J. McClellan, M. R. Levy, C. Milanese, R. W. Grimes, *Nucl. Instrum. Methods Phys. Res. A,* 2007, **579**, 27–30.

Published on 04 March 2021. Downloaded by Université Claude Bernard Lyon on 3/10/2021 9:05:29 AM.

CrystEngComm Accepted Manuscript